Nonlinear Dyn (2014) 77:1485–1502
DOI 10.1007/s11071-014-1393-2

ORIGINAL PAPER

A locomotive's dynamic response to in-service parameter variations of its hydraulic yaw damper

W. L. Wang · D. S. Yu · Y. Huang · Z. Zhou · R. Xu

Received: 8 September 2013 / Accepted: 23 March 2014 / Published online: 11 April 2014

Abstract An improved hydraulic yaw damper model with series in-service clearance and comprehensive stiffness was proposed by Wang et al. (Nonlinear Dyn 65(1–2):13–34 2011). In order to study how in-service parameter variations to the hydraulic yaw damper affect the dynamics of a Chinese SS_9 locomotive, this study continued that research by establishing a multibody system (MBS) model of the SS_9 locomotive–rail coupling system, and then validating the MBS model using field test data from the SS_9. Extensive simulations were performed, and the results demonstrated that both the effective stiffness and the small clearance accumulated between two ends of the damper due to wear and lack of maintenance had remarkable impacts on the locomotive's critical speed and on its normal operation. The results also influenced the locomotive's ride comfort, but the effect of the small clearance was more remarkable than that of the effective stiffness in this regard, and these parameters had little to no influence on the locomotive's curve-negotiation performance. The small clearance and effective stiffness are usually omitted or simplified in engineering, and so it was important to apply the proposed in-service nonlinear damper model with series clearance and stiffness to a vehicle dynamics study and improve the accuracy of vehicle design. The study was also useful for setting pertinent vehicle maintenance standards in engineering to control the influence of such in-service parameter variations.

Keywords Locomotive dynamics · Hydraulic yaw damper · In-service parameter · Effective stiffness · Small clearance

W. L. Wang (✉) · D. S. Yu · Z. Zhou · R. Xu
College of Mechanical and Vehicle Engineering, Hunan University, Changsha 410082, People's Republic of China
e-mail: pianowwl@163.com

W. L. Wang
The State Key Laboratory of Fluid Power Transmission and Control, Zhejiang University, Hangzhou 310027, People's Republic of China

Y. Huang
The State Nuclear Power Engineering Company, Shanghai 200233, People's Republic of China

1 Introduction

Hydraulic yaw dampers are widely used in modern train systems to achieve lateral stability in the vehicles. As shown by Fig. 1, a locomotive hydraulic yaw damper is situated horizontally and longitudinally between the bogie and the carbody, designed to act as a hydraulic friction [1] damping device to attenuate the components' relative yaw motions. In normal circumstances, each vehicle has two bogies, and each bogie has two yaw dampers.

The dynamic stability [2,3] of a rail vehicle has many influential factors, such as the nonlinear wheel–rail contact and creep forces [4–6], the suspension parameters [7,8] and even the vehicle's inertial properties [9]. The hydraulic yaw damper, however, is a key

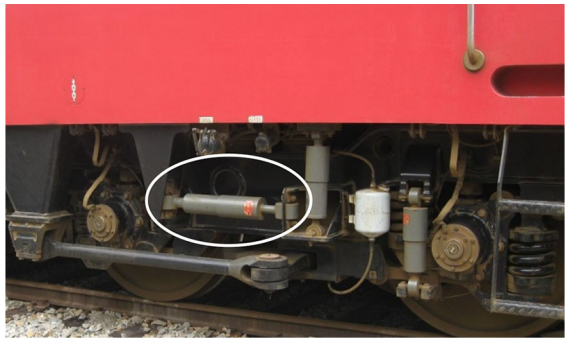

Fig. 1 A locomotive hydraulic yaw damper in service

component of dynamic stability. Fujimoto et al. [10] employed hydraulic yaw dampers to mitigate severe hunting motions and lateral vibrations in a Shinkansen train and suggested ways to improve the effective damping coefficient and stiffness of the yaw damper by increasing the oil elastic modulus and the rubber attachment stiffness and designing the piston diameter to be as large as possible. Wrang [11] improved the critical speed of a passenger coach by 15–25 km/h and eliminated its instable running phenomena by increasing the rubber attachment stiffness of its hydraulic yaw damper. During troubleshooting, it was concluded that small in-service parameter variations in the key components could lead to remarkable vehicle dynamics responses. Mellado et al. [12] found that the effective stiffness of a yaw damper decreased remarkably if the damper was exposed to small displacement excitations, which are very common in rail vehicles, so they corrected the damper model using bench test results. However, a test bench's damper performance is very different from that in service, meaning that a decrease in the effective stiffness may be the result of many factors, such as the small clearance between a yaw damper and its mounting seats, the actual oil elastic modulus or the mounting seat stiffness. Piao et al. [13] simulated the dynamic stability behaviour of a Chinese high-speed CRH_3 train by assuming that one of its yaw dampers was experiencing failure. These studies showed that when a hydraulic yaw damper was subject to small displacement excitations in real scenarios, a variety of parameter variations that are usually omitted in experiments could be crucial to its normal functioning. Therefore, the effects of in-service parameter variations made to the hydraulic yaw damper on vehicle dynamics required further careful study and understanding.

Multibody system (MBS) modelling and simulation [14,15] is commonly used in modern rail vehicle studies [16–18], virtual prototyping [19] and structural designs [20]. Several commercial software packages are available and employed in such studies, including DynaRail [21], ADAMS/Rail [18] and SIMPACK [15–17,19,20,22,23].

Reference [1] proposed an improved damper model with in-service series clearance and comprehensive stiffness. The model improved upon the Maxwell model described in the European Standard [24], and the authors also provided detailed nonlinear parametric modelling and parameter sensitivity analysis of the hydraulic yaw damper used in Chinese SS_9 locomotives and uncovered how the in-service parameters affected the damper's macro-damping performance. This paper continues the research in reference [1] and addresses the issue of how the yaw damper's in-service parameters affect locomotive dynamics.

The MBS modelling of a Chinese SS_9 locomotive is conducted in the SIMPACK environment, after which the established model is validated using field test data collected for the SS_9. Extensive simulations are performed to predict the effects of in-service parameter variations made to the hydraulic yaw damper on the locomotive's dynamics. The results show that both the effective stiffness and the small clearance have remarkable impacts on the locomotive's critical speed and even on its normal operation, and also influence the locomotive's ride comfort. However, the effect of small clearance is more remarkable than that of effective stiffness, and these parameters have little or no influence on the locomotive's curve-negotiation performance.

The small clearance and the effective stiffness are usually omitted or simplified in engineering, and so the in-service nonlinear damper model with series clearance and stiffness proposed in [1] is suggested for the study of vehicle dynamics and the improved accuracy of vehicle design. Pertinent vehicle maintenance standards should also be set to control the influence of such in-service parameter variations in industry.

2 MBS modelling and validation

2.1 MBS model of the locomotive–rail coupling system

SS_9 [25] is one of the main Chinese electric locomotives in use today. It has a C_0–C_0 axle style, and a

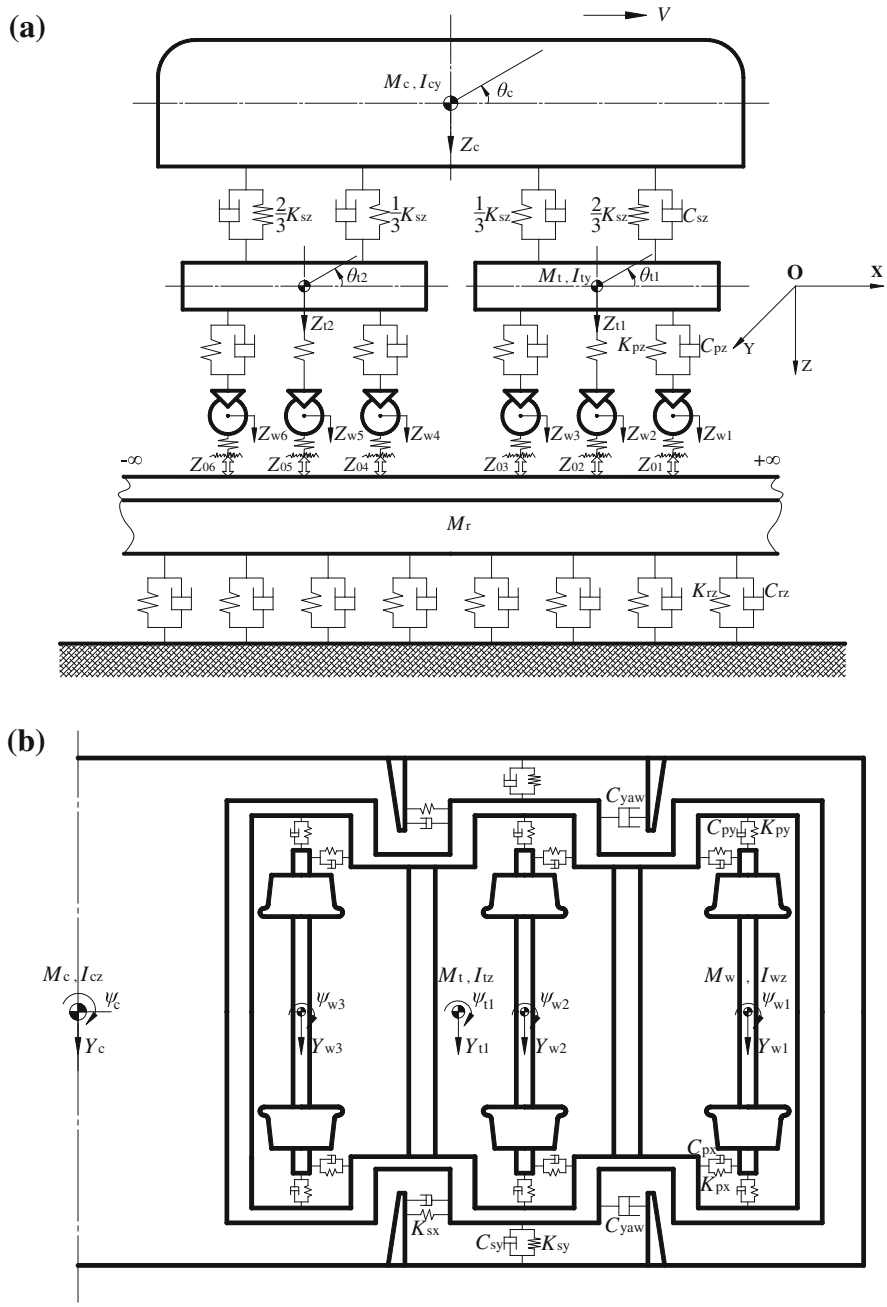

Fig. 2 Physical model of the SS_9 locomotive–rail coupling system: **a** Front view, **b** bird's-eye view and **c** back view

physical model of the SS_9's locomotive–rail coupling system is demonstrated in Fig. 2. The locomotive has two bogies, and each bogie has three axles (wheelsets), while the primary suspension supplies stiffness and damping between the wheelsets and the bogie frame in the longitudinal, lateral and vertical directions, and so does the secondary suspension supply between the bogie frame and the carbody. The total degrees of freedom (DOFs) in the locomotive system are listed in Table 1.

The railroad model is a simplified and effective model that can be illustrated by the drawings in Fig. 2a, c. M_r is a continuous effective mass that includes the steel rails, sleepers and the vibrating fraction of the roadbed, and it is distributed longitudinally. K_{ry} is the lateral stiffness, produced mainly by the rail fasten-

Fig. 2 continued

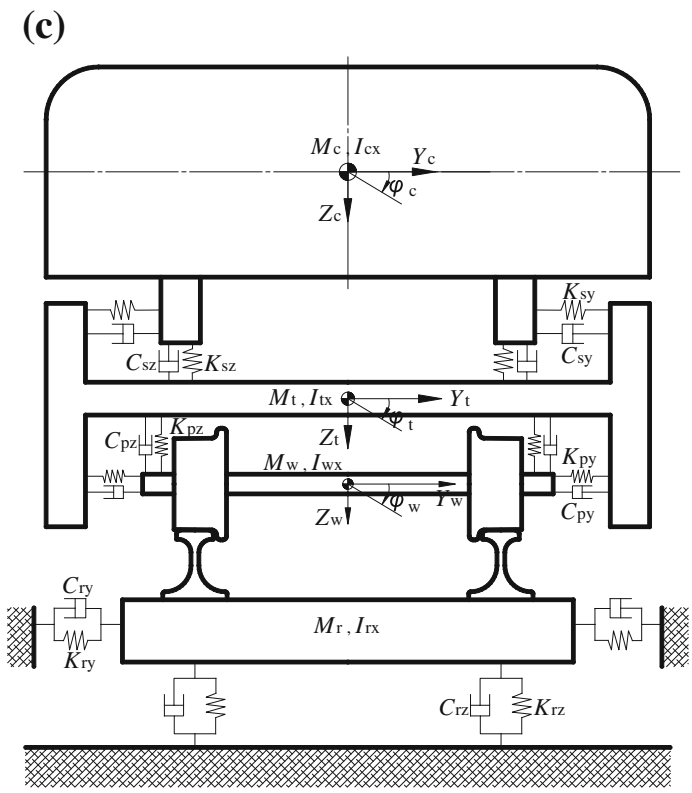

Table 1 DOFs of the locomotive system

	Longitudinal displacement	Lateral displacement	Vertical displacement	Roll angle	Pitch angle	Yaw angle
Carbody	–	Y_c	Z_c	ϕ_c	θ_c	ψ_c
Bogie frame ($i = 1, 2$)	–	Y_{ti}	Z_{ti}	ϕ_{ti}	θ_{ti}	ψ_{ti}
Wheelset ($i = 1$–6)	–	Y_{wi}	Z_{wi}	ϕ_{wi}	θ_{wi}	ψ_{wi}

ers, and C_{ry} is a comprehensive damping coefficient. K_{rz}, however, is the parallel result of the vertical stiffness produced by the rail fasteners, the rubber rail-pad stiffness, and the roadbed stiffness, and C_{rz} is also a comprehensive damping coefficient.

The JM3 worn wheel profile and the 60 kg/m Chinese standard rail profile [3,25] are used in the wheel–rail contact model, while the simplified Kalker's law [2,3] is employed to calculate the creep forces. American sixth grade track profiles (Am6) can be used as track inputs for Chinese trunk line conditions [26,27], and the spectrum density function for the rail's vertical and alignment profile is given by

$$S_v(\Omega) = S_a(\Omega) = \frac{5.7613 \times 10^{-3}}{\Omega^2\left(\Omega^2 + 0.6798\right)}, \quad (1)$$

while that for the rail's cross level and gauge profile is given by

$$S_c(\Omega) = S_g(\Omega) = \frac{2.3045 \times 10^{-2}}{\left(\Omega^2 + 0.6798\right)\left(\Omega^2 + 0.1918\right)}. \quad (2)$$

where $\Omega = 2\pi f$ is the spatial frequency in (rad/m) and $S(\Omega)$ is the spectrum density in [cm^2/(rad/m)].

A MBS model of the SS_9 locomotive-rail coupling system is established in the SIMPACK environment based on this physical model. The final MBS model is shown in Fig. 3 and the pertinent parameters and their values are given in the Appendix.

2.2 Model validation

A nominal force calculation shows that the acceleration of the MBS model in its equilibrium state is 7.568E−5 m/s^2, which is far less than the evaluation

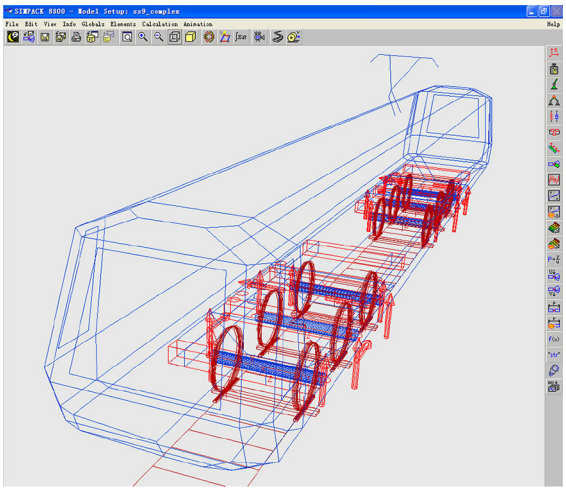

Fig. 3 MBS model of the SS_9 locomotive–rail coupling system established in the SIMPACK environment

criteria of 1E−4 m/s^2 [28], indicating that the proposed MBS model is accurate. The SS_9 dynamics are then simulated using the above MBS model. Figure 4 shows the lateral vibrations of the No. 1 wheelset, the front bogie frame and the carbody, while the locomotive operates on a tangent track at the speed $V = 160$ km/h. Figure 4 shows that the simulation results are rational because the vibration of the wheelset is more intense than that of the bogie frame, while the vibration of the bogie frame is more intense than that of the carbody.

Figure 5 gives a graphical comparison of field test data [29] (dotted line) with the simulation results (solid line) for the SS_9 dynamics. Figure 5a demonstrates that both the field test results and the simulation results have the same increasing trend when the locomotive speeds up, but the field test results are larger than those of the simulation to some extent. This difference might occur because actual rail excitations are more intense than those of the Am6 rail excitation input in the simulation. A more detailed comparison, however, shows that the mean relative errors for the carbody's lateral and vertical vibrations are 10.12 and 14.83 %, respectively, both of which are smaller than the allowable criteria of 15%. A comparison of the data shown in Fig. 5b also confirms that the mean relative errors for the lateral and vertical ride comfort indices are 6.58 and 1.44 %, respectively, indicating that the simulation results are very accurate.

A similar comparison is also performed for the curving behaviour of the locomotive and illustrates the MBS simulation's accuracy. Thus, the MBS model established for the SS_9 locomotive dynamics simulation is validated and proven effective for the next step in the study, involving the prediction of in-service parameter effects.

3 Dynamic response and discussion

3.1 Research method

Because the damping characteristics defined by the full parametric model [1] have more than 60 parameters and intrinsically minor nonlinearities, coupling the full parametric damper model into the MBS dynamics calculation is not only unwieldy but also not cost-

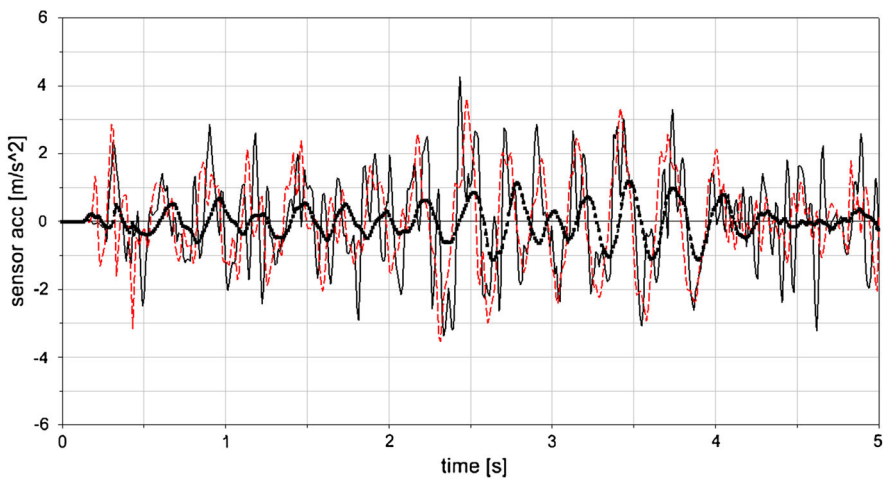

Fig. 4 Lateral vibration accelerations of the No. 1 wheelset, the front bogie frame and the carbody (*black solid line* No. 1 wheelset, *red dotted line* front bogie frame, *black dotted-dashed line with markers* carbody; simulation condition $V = 160$ km/h on the tangent track)

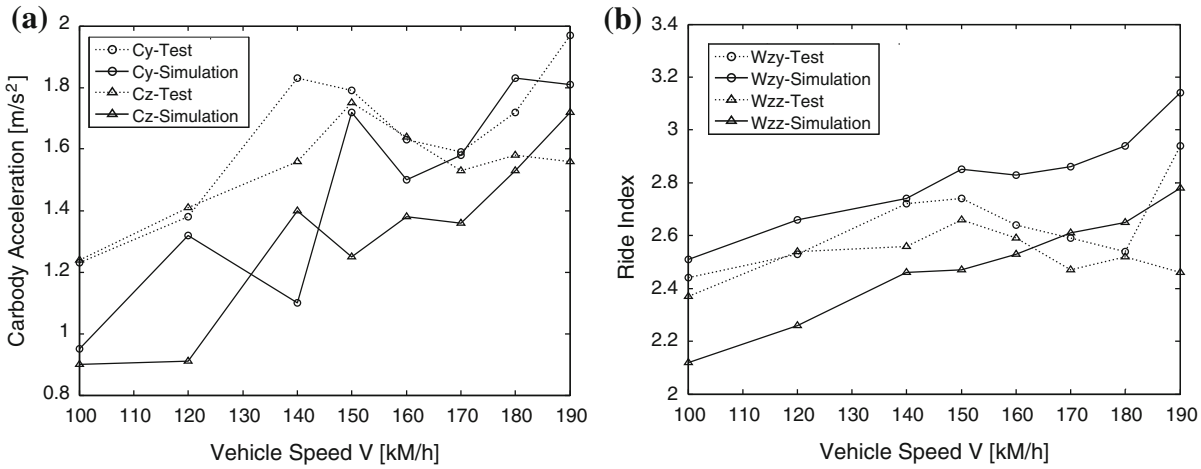

Fig. 5 Comparison of field test data with the simulation results: **a** carbody vibration accelerations (C_y: lateral, C_z: vertical) and **b** ride comfort indices (W_{zy}: lateral, W_{zz}: vertical)

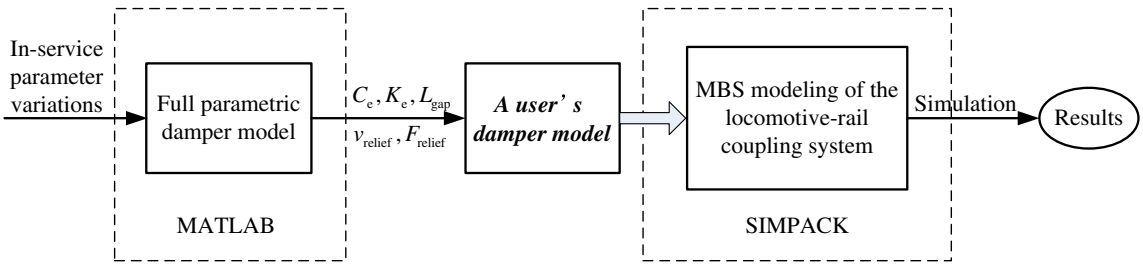

Fig. 6 The flow chart for predicting a locomotive's dynamic response to in-service parameter variations made to its hydraulic yaw damper

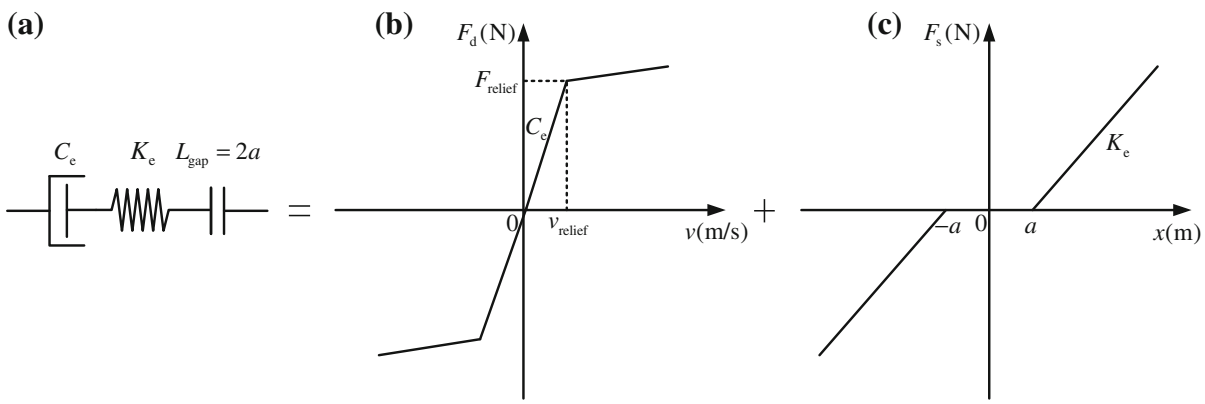

Fig. 7 Implementation of the in-service hydraulic damper model to a user's damper model in the MBS modelling: **a** In-service hydraulic damper model, **b** effective nonlinear damping and **c** effective stiffness with clearance

effective. Figure 6 shows the research method for predicting a locomotive's dynamic response to in-service parameter variations made to its hydraulic yaw damper. It consists of estimating C_e, K_e, $2a$, v_{relief} and F_{relief} using the full parametric model in [1], defining a user's damper model in MBS modelling and calculating the dynamic response using the MBS model established in this study.

Figure 7 shows the concrete implementation of an in-service hydraulic damper model [1] to a user's damper

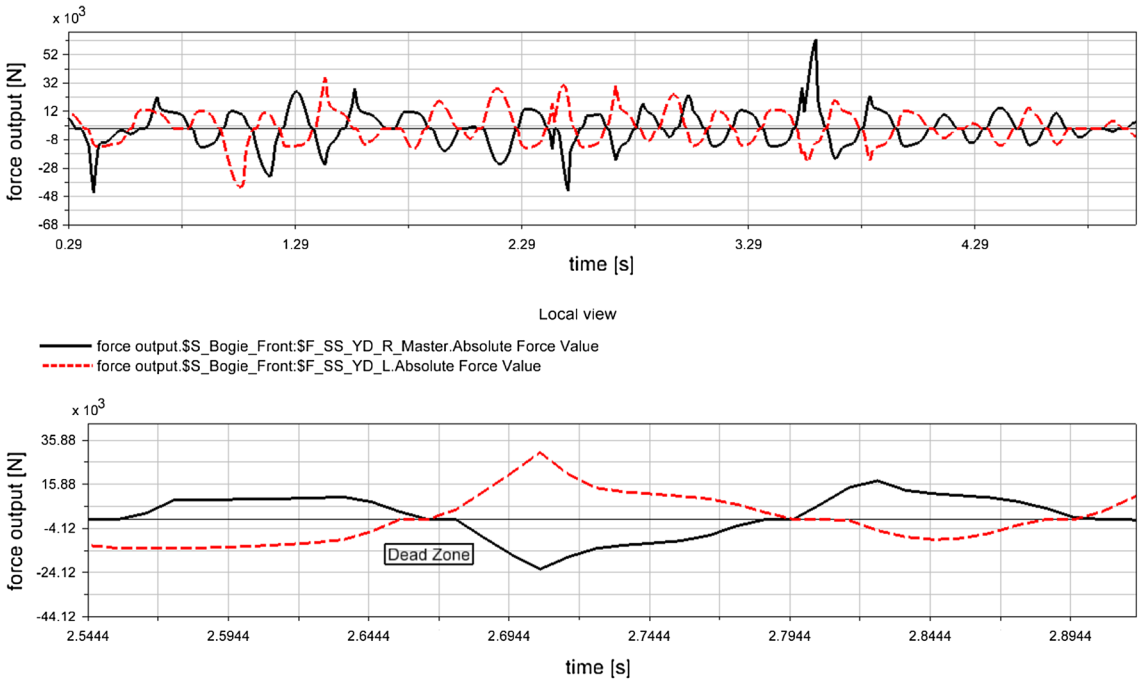

Fig. 8 Damping force profiles of the left and right hydraulic yaw dampers on the front bogie (*black solid line* left yaw damper, *red dotted line* right yaw damper; simulation conditions: $C_e = 1,000$ kNs/m, $K_e = 1.1E{+}007$ N/m, $2a = 1$ mm and $V = 160$ km/h on the tangent track)

model in the SS_9 MBS modelling. In Fig. 7a, C_e is the effective damping coefficient, which is affected by the oil pressure, oil temperature and entrained air ratio; K_e is the tandem result of the rubber attachment stiffness (K_{rubber}), the oil spring stiffness (K_{oil}, also affected by the oil pressure, oil temperature and entrained air ratio) and the mounting seat stiffness (K_{seat}) [30]; $L_{gap} = 2a$ is the small clearance between the damper and its mounting seats (affected by the structural clearance, wear, loosening and maintenance), and $L_{gap} = 2a = 1$ mm is common in normal engineering practice; v_{relief} and F_{relief} are the critical velocity and damping force, respectively, when the hydraulic yaw damper is relieved, or in other words, when the hydraulic friction damping force gets saturated.

All the in-service hydraulic dampers in the SS_9 MBS model (including the hydraulic yaw dampers) are defined as point-to-point spring–damper serial force elements. In other words, the user's hydraulic damper model is defined as the result of both the effective nonlinear damping depicted in Fig. 7b and the effective stiffness with clearance depicted in Fig. 7c.

Figure 8 shows the simulated damping force profiles of the left and right hydraulic yaw dampers on the front bogie under normal damper conditions. The curve at the top of Fig. 8 shows that the left and right yaw dampers work cooperatively to damp the locomotive's yaw motions: one pushes and the other drags. During normal operations, each hydraulic yaw damper works at a frequency of approximately 3.5 Hz and a mean magnitude of ±3–4 mm.

The curve at the bottom of Fig. 8 represents an enlarged local view of the top curve and clearly shows that, due to the small clearance between the damper and its mounting seats, the damping force profiles exhibit not only dead zones but also inertial impacts when the dampers change their directions.

3.2 Nonlinear dynamic stability

3.2.1 Critical locomotive speed in good conditions

To obtain the locomotive's critical speed, the No. 4 wheelset (i.e., the No. 1 wheelset of the rear bogie) is

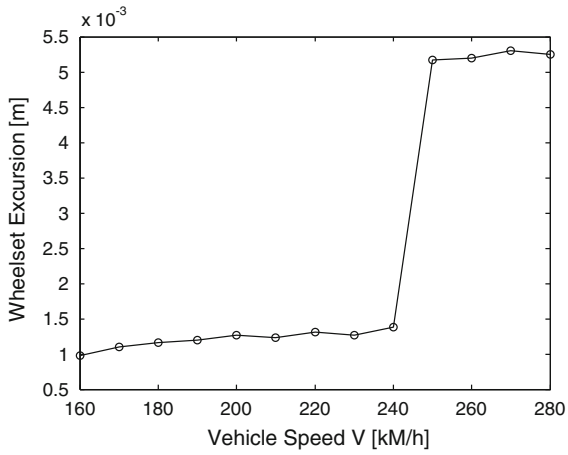

Fig. 9 Stable lateral excursion of the No. 4 wheelset at different vehicle speeds (simulation conditions: $C_e = 1,000$ kNs/m, $K_e =$ 1.25E+007 N/m and $2a = 0.2$ mm)

excited by 3 mm initial lateral excursion [28] while the locomotive is running on a tangent track under Am6 rail irregularity excitations. The stable response of the No. 4 wheelset's lateral vibration is then observed. A simulation is performed when the locomotive (including its hydraulic yaw dampers) is in good condition, the result of which is shown in Fig. 9.

Figure 9 shows that the lateral vibration response of the No. 4 wheelset is convergent at a vehicle speed range of V =160–240 km/h in good conditions. The constant amplitude lateral vibration, however, occurs abruptly at a vehicle speed: $V = 250$ km/h. In other words, the limit cycle of the No. 4 wheelset lateral vibration occurs at $V = 250$ km/h, and when the vehicle speed exceeds this value, the No. 4 wheelset's lateral vibration diverges. Thus, it is concluded that the SS_9 locomotive's critical speed under good conditions equals 250 km/h.

3.2.2 *Effect of in-service parameter variations to the hydraulic yaw damper on the locomotive's critical speed*

Figure 10 demonstrates the simulation results for the effect of in-service parameter variations to the hydraulic yaw damper on the locomotive's critical speed. Figure 10a shows that increasing the effective stiffness K_e of the hydraulic yaw damper from 3 to 15 MN/m increases the locomotive's critical speed from 212 to 260 km/h. In other words, the locomotive's critical speed is improved by 22.6 %.

The effective stiffness K_e of a hydraulic yaw damper is determined by a combination of its rubber attachment stiffness K_{rubber} and the intrinsic oil spring stiffness of the damper, which can be quite low because of the long stroke needed to accommodate curving. The oil temperature and entrained air ratio also affects K_e, but their effects are limited [1]. Thus, a hydraulic yaw damper's rubber attachment should be made stiffer to gain better dynamic stability. However, considering the drawbacks

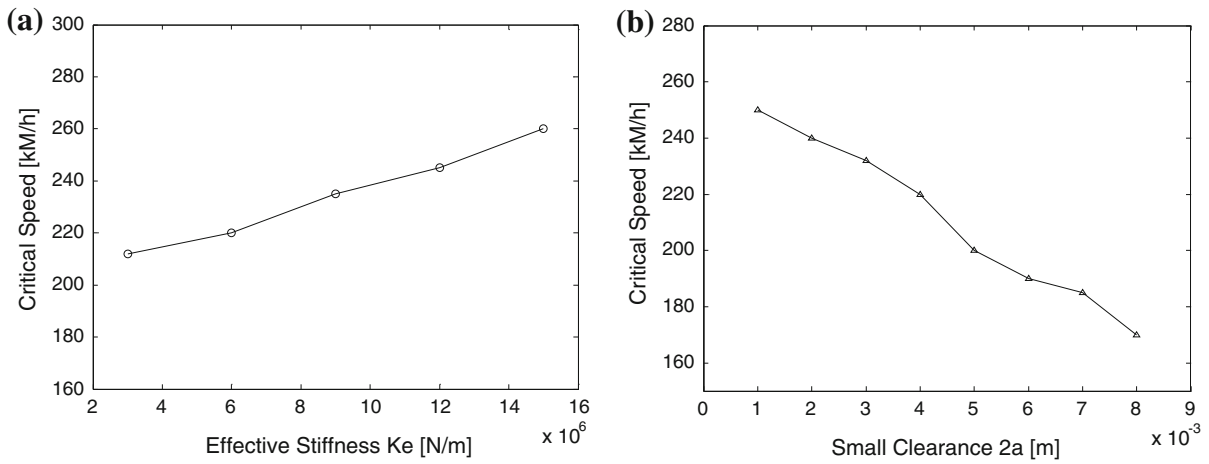

Fig. 10 Effect of in-service parameter variations to the hydraulic yaw damper on the locomotive's dynamic stability (critical speed): **a** effect of effective stiffness on critical speed (simulation conditions: $C_e = 1,000$ kNs/m and $2a = 0.2$ mm) and **b** effect of small clearance on critical speed (simulation conditions: $C_e = 1,000$ kNs/m and $K_e =$ 1.25E+007 N/m)

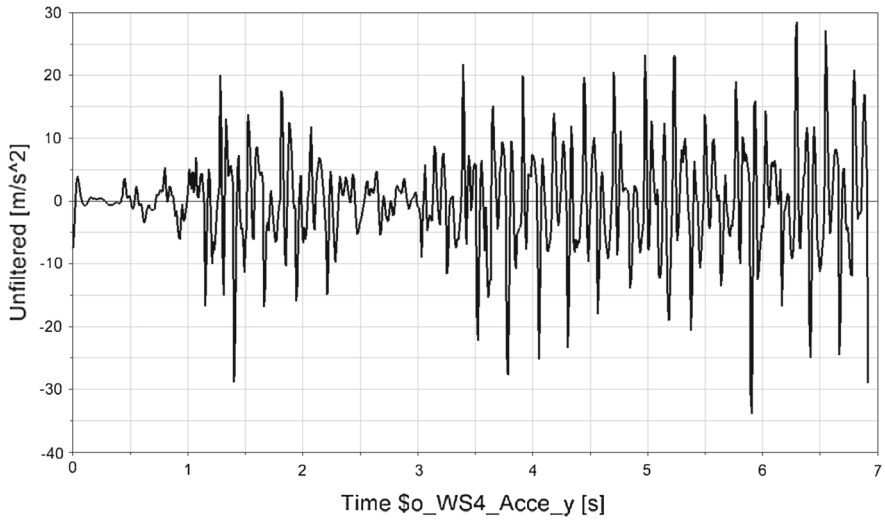

Fig. 11 Divergence of the No. 4 wheelset's lateral vibration (simulation conditions: $2a = 8$mm, $C_e = 1{,}000$ kNs/m, $K_e =$ 1.25E+007 N/m and $V =$ 170 km/h on the tangent track)

of transferring high-frequency vibrations, the rubber attachment stiffness value K_{rubber} should also not be set too high.

Figure 10b shows that increasing the hydraulic yaw damper's small clearance $2a$ (refer to Fig. 7c) from just 1 to 8 mm would decrease the locomotive's critical speed from 250 to 170 km/h. In other words, the locomotive's critical speed is decreased remarkably by 32 %. This result is not difficult to explain. A rail vehicle's vibration is a type of typical high-frequency, low-amplitude vibration. For example, when an SS_9 locomotive operates at the speed V=160 km/h, the working frequency of its hydraulic yaw damper is approximately 3.5 Hz and its mean working amplitude is approximately ±3.46 mm. Thus, if the small clearance factor a reaches 3–4 mm ($L_{\text{gap}} = 2a$ = 6–8 mm), the hydraulic yaw dampers are simply suspended and are not in service (i.e. they are non-functioning). Figure 11 shows the simulated divergent performance (instability) of the No. 4 wheelset's lateral vibration when the small clearance a reaches 4 mm.

A structural clearance of approximately 1 mm between the hydraulic yaw damper and its mounting seats exists in practice. The total clearance $2a$ may also reach 2–3 mm or more due to wear, loosening, or lack of maintenance, and the influence of the small clearance $2a$ on the locomotive's dynamic stability would be significant in this case. Thus, the small clearance, which is not readily noticeable in design or engineering maintenance, could contribute significantly to a vehicle's dynamic response.

Therefore, the effective stiffness K_{e} and the small clearance $2a$ of the in-service hydraulic yaw damper has a remarkable impact on the SS_9 locomotive's critical speed, with a magnitude of 22–32 %, which obviously affects the locomotive's normal operation.

A similar study is concerned with the influence of yaw damper's oil temperature and entrained air ratio on the locomotive's critical speed, and shows that this influence is not obvious under normal operations. Because the increase in the oil temperature and entrained air ratio would weaken the yaw damper's damping coefficient, it could exert more or less influence on the vehicle's lateral vibrations. However, the study's result also shows that such influence is limited.

3.3 Ride comfort

3.3.1 Effect of effective stiffness variation in the hydraulic yaw damper on the locomotive's ride comfort

Figure 12 demonstrates the effect of the study's effective stiffness variation in the hydraulic yaw damper on the lateral vibration of the front bogie frame. The figure shows only two curves for $K_{\text{e}} =$ 3E+006 and $K_{\text{e}} =$ 1.5E+007 N/m to ensure clarity, and indicates that increasing the effective stiffness would mitigate lateral vibration in the front bogie frame.

Figure 13 demonstrates the effect of varying K_{e} in the hydraulic yaw damper on the power spectrum

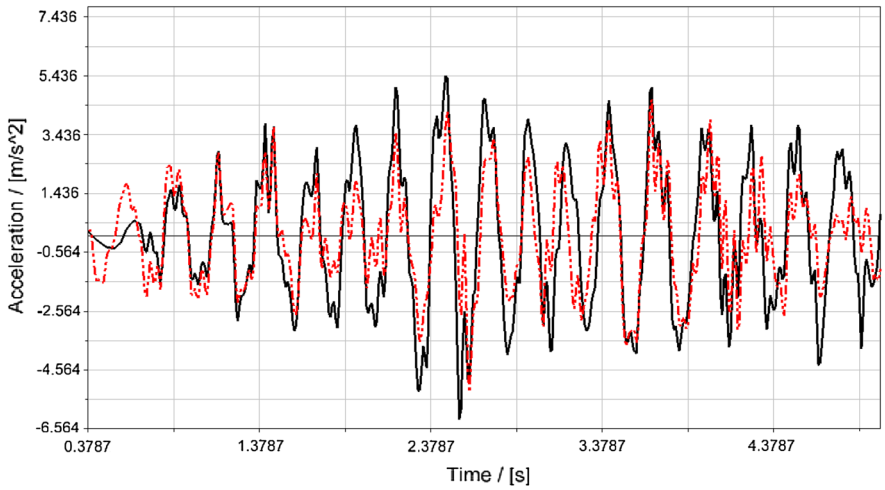

Fig. 12 Effect of effective stiffness variation in the hydraulic yaw damper on the front bogie frame's lateral vibration (*black solid line* K_e = 3E+006 N/m, *red dotted line* K_e = 1.5E+007 N/m; simulation conditions: C_e = 1,000 kNs/m, $2a$ = 1 mm and V = 160 km/h on the tangent track)

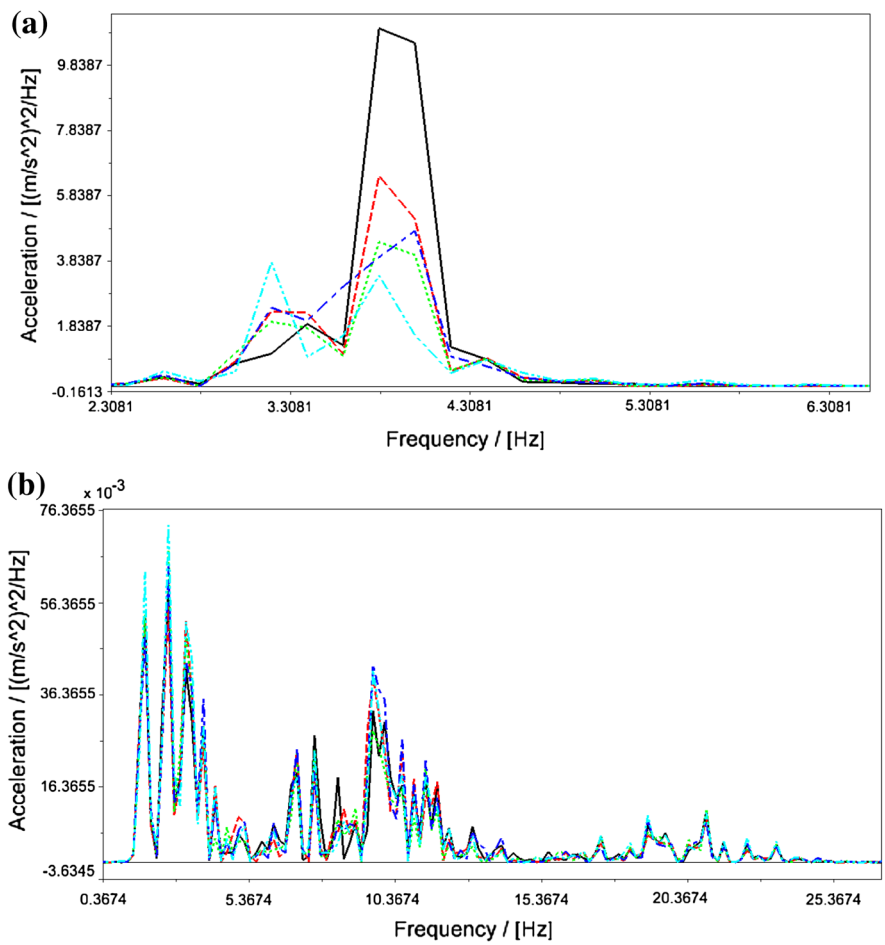

Fig. 13 Effect of effective stiffness variation in the hydraulic yaw damper on the power spectrum density (PSD) of the front bogie frame's vibrations: PSD of **a** the lateral vibration and **b** the vertical vibration (*black solid line* K_e =3E+006 N/m, *red dotted line* K_e = 6E+006 N/m, *green dotted line* K_e = 9E+006 N/m, *blue dotted-dashed line* K_e = 1.2E+007 N/m, *cyan dotted-dashed line* K_e = 1.5E+007 N/m; simulation conditions: C_e = 1,000 kNs/m, $2a$ = 1 mm and V = 160 km/h on the tangent track)

density (PSD) of the front bogie frame's vibrations. Figure 13a shows that lateral vibration of the front bogie frame has two mode frequencies at 3.2 Hz and 3.8 Hz. As K_e increases, the hydraulic yaw damper dissipates the vibration energy more significantly at the main frequency of 3.8 Hz, with the macro effect

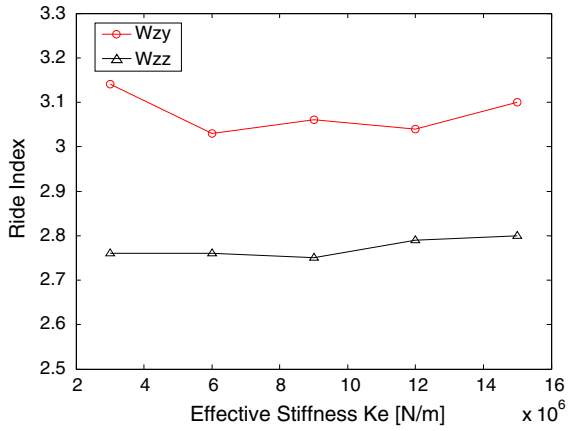

Fig. 14 Effect of effective stiffness variation in the hydraulic yaw damper on the SS_9 locomotive's ride comfort (W_{zy}: lateral ride index, W_{zz}: vertical ride index; simulation conditions: C_e = 1,000 kNs/m, $2a$ = 1 mm and V = 160 km/h on the tangent track)

of the lateral vibration in the front bogie frame being reduced more significantly. Figure 13a also shows that the hydraulic yaw damper's vibration reduction ability weakens gradually and moderately with the increase in K_e at the frequency of 3.2 Hz. However, 3.2 Hz is not the main mode frequency and makes a smaller contribution to the macro-lateral vibration. Figure 13b shows that the effect of varying K_e on the front bogie frame's vertical vibration performance is not significant.

A similar study is concerned with the effect of K_e variations on the car body's vibration performance. This research concludes that as K_e increases, the hydraulic yaw damper will dissipate the car body's lateral vibrations more significantly, but will have no obvious influence on its vertical vibrations.

Figure 14 gives the calculated results of the K_e variations on the SS_9 locomotive's ride comfort and concludes that the effective stiffness variation has a moderate influence on the locomotive's lateral ride index. With a properly designed effective stiffness, the hydraulic yaw damper could be useful for achieving better lateral ride comfort, but if the effective stiffness were too soft or hard, then it would worsen the lateral ride comfort. Variations to the effective stiffness have no obvious influence on the locomotive's vertical ride index. Figure 14 also indicates that when the SS_9 operates at 160 km/h, its lateral ride index reaches the 'good' benchmark, and its vertical ride index reaches the 'excellent' benchmark [31].

3.3.2 *Effect of small clearance variations in the hydraulic yaw damper on the locomotive's ride comfort*

Figure 15 demonstrates the effect of small clearance variations in the hydraulic yaw damper on the car body's lateral vibration. For simplicity, the figure gives only two curves representing $2a$ = 0.5 mm and $2a$ = 4 mm. Figure 15 shows that the car body's lateral vibration is intensified remarkably when the small clearance $2a$ increases from 0.5 to 4 mm.

Figure 16 illustrates the effect of small clearance variations in the hydraulic yaw damper on the carbody's lateral vibration PSD, showing that with the increase in $2a$, the vibration-reduction ability of the hydraulic

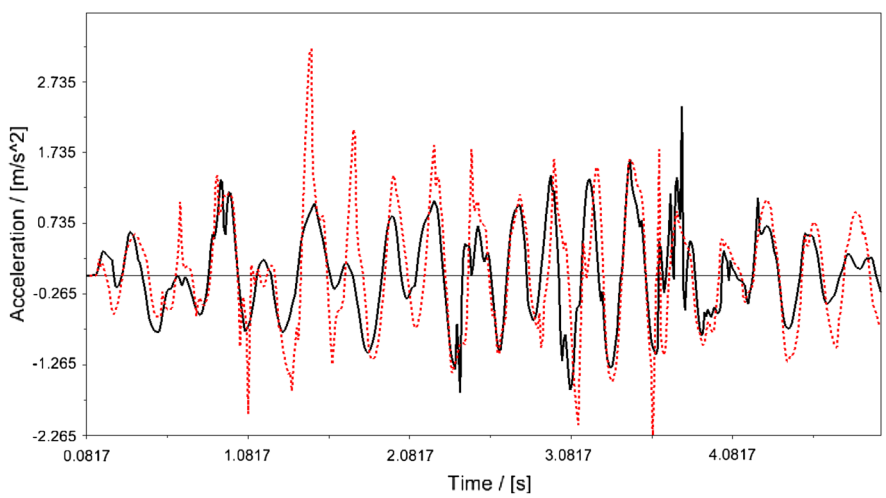

Fig. 15 Effect of small clearance variations in the hydraulic yaw damper on the car body's lateral vibration (*black solid line* $2a$ = 0.5 mm, *red dotted line* $2a$ = 4 mm; simulation conditions: C_e = 1,000 kNs/m, K_e = 1.25E+007 N/m and V = 160 km/h on the tangent track)

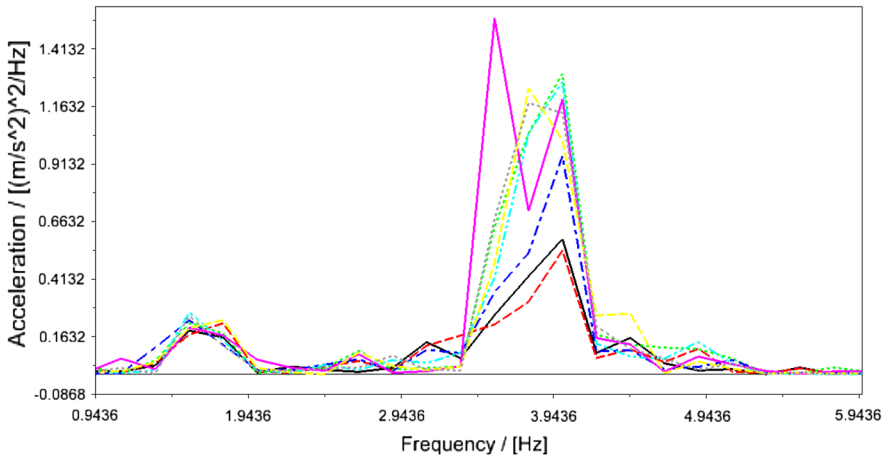

Fig. 16 Effect of small clearance variations in the hydraulic yaw damper on the PSD of the carbody's lateral vibration (*black solid line* $2a = 0.5$ mm, *red dotted line* $2a = 1$ mm, *green dotted line* $2a = 1.5$ mm, *blue dotted-dashed line* $2a = 2$ mm, *cyan dotted-dashed line* $2a = 2.5$ mm, *pink solid line*: $2a = 3$ mm, *yellow dotted line* $2a = 3.5$ mm, *gray dotted line* $2a = 4$ mm; simulation conditions: C_e=1,000 kNs/m, $K_e = 1.25$E+007 N/m and $V = 160$ km/h on the tangent track)

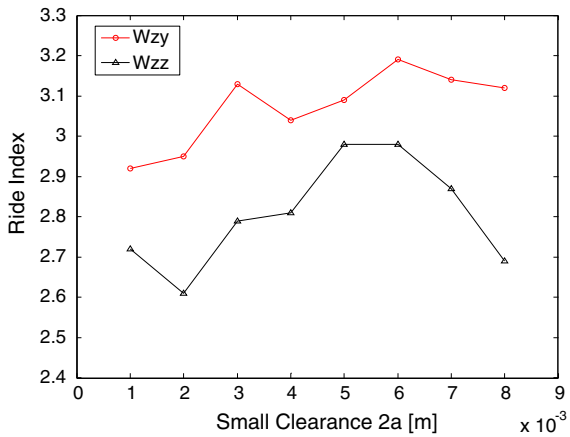

Fig. 17 Effect of small clearance variations in the hydraulic yaw damper on the SS_9 locomotive's ride comfort (W_{zy}: lateral ride index, W_{zz}: vertical ride index; simulation conditions: $C_e = 1{,}000$ kNs/m, $K_e = 1.25$E+007 N/m and $V = 160$ km/h on the tangent track)

yaw damper weakens gradually at the car body's main mode frequency (approximately 3–4 Hz). Beyond the main mode frequency, however, the influence of small clearance variation on the car body's lateral vibration energy distribution is not obvious.

A similar exercise is performed, which concludes that small clearance variation has no obvious influence on the car body's vertical vibration.

Figure 17 shows the calculated effect of small clearance variations in the hydraulic yaw damper on the SS_9 locomotive's ride comfort. The figure indicates that small clearance variations have an obvious influence on both the lateral and vertical ride indices of the locomotive. Within the range of 1–6 mm, increasing the small clearance $2a$ increases both the lateral and vertical ride indices, which means that both the lateral and vertical ride comforts of the locomotive deteriorate because, as the small clearance increases, the hydraulic yaw damper's vibration-reduction ability gradually weakens. On the other hand, the locomotive's ride comfort also deteriorates due to the dead-zone-induced inertial impacts when the damper changes its direction.

When exceeding 6 mm, however, the small clearance is equal to or larger than the working amplitude of the hydraulic yaw damper, suspending it at that value, and most of its inertial impacts are eliminated. Both the lateral and vertical ride indices of the locomotive decrease as a result, as shown in Fig. 17.

Comparing Fig. 17 with Fig. 14, it can be concluded that the effect of small clearance on the locomotive's ride comfort is larger than that of effective stiffness. Not only does the small clearance couple lateral and vertical vibrations to some extent, but it also deteriorates the ride comfort to a remarkable extent. As shown in Figs. 17 and 14, the small clearance effect degrades the lateral ride index from a 'good' to a 'qualified' level, and it decreases the vertical ride index from an 'excellent' to a 'good' level [31].

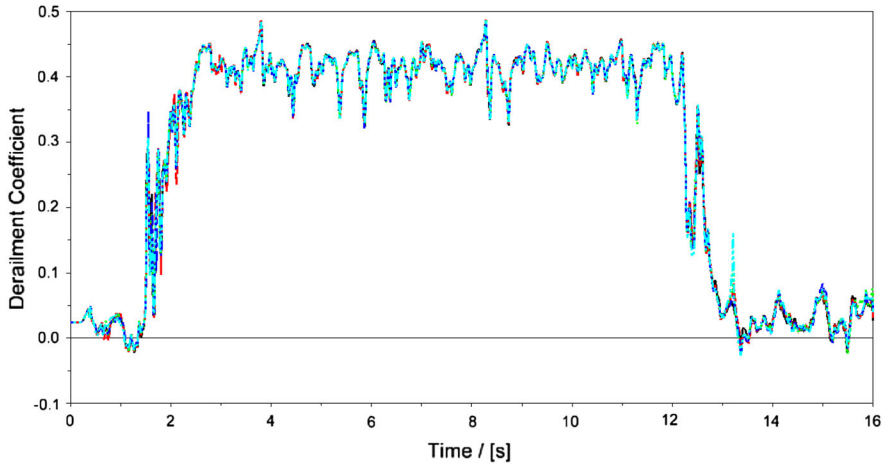

Fig. 18 Effect of varying the hydraulic yaw damper's effective stiffness on the derailment coefficient of the No. 1 wheelset (*black solid line* K_e = 3E+006 N/m, *red dotted line* K_e = 6E+006 N/m, *green dotted line* K_e = 9E+006 N/m, *blue dotted-dashed line* K_e = 1.2E+007 N/m, *cyan dotted-dashed line* K_e = 1.5E+007 N/m; simulation conditions: C_e = 1,000 kNs/m, $2a$ = 1 mm, V = 80 km/h on a curved track, curve radius is 400 m and outer rail super-elevation is 0.12 m)

3.4 Curve-negotiation performance

The SS_9 locomotive's dynamic curve-negotiation response is simulated when the vehicle operates on a curved track at the speed V = 80 km/h and with Am6 track irregularity excitations. The curve radius is 400 m, and the outer rail's super-elevation is 0.12 m. The simulation results show that both the effective stiffness and the hydraulic yaw damper's small clearance variation have hardly any influence on the derailment coefficient or wear power of the wheelsets. As an example, Fig. 18 shows the effect of varying K_e on the derailment coefficient of the No. 1 wheelset.

An extensive simulation is also performed to study the effects of in-service parameter variations in the hydraulic yaw damper on the lateral shift force of the wheelsets. This simulation shows that increasing both the effective stiffness and the small clearance increases the lateral shift force of the wheelsets, but these increases are limited.

As an example, Fig. 19 shows the effect of $2a$ variation on the lateral shift performance of the No. 1 wheelset. For simplicity, the figure shows only two curves, when $2a$ = 0.5 mm and $2a$ = 4 mm. Figure 19a illustrates that increasing the small clearance will moderately increase the lateral shift force of the wheelset because as the clearance increases, the hydraulic yaw damper becomes less restrictive on the locomotive's curve negotiation and increases the lateral shift. Therefore, the lateral shift force of the wheelsets also increases. The above phenomena can also be explained by a Bode plot of the lateral shift force, as shown in Fig. 19b. As clearance increases, the hydraulic yaw damper's ability to transfer the lateral shift force of the wheelsets increases to some extent over the full frequency range.

4 Conclusion

When a hydraulic damper is subjected to high-frequency, small-displacement excitations in the real world, its in-service parameter variations can be crucial to its normal functioning and thus affect the vehicle's dynamics in remarkable ways. This study conducts MBS modelling and dynamic response prediction of a Chinese SS_9 locomotive based on in-service parameter variations made to its hydraulic yaw damper. The following conclusions can be drawn as a result of this study.

(1) An increase in the effective stiffness K_e of the hydraulic yaw damper from 3 to 15 MN/m leads to an increase in the locomotive's critical speed from 212 to 260 km/h. An increase in the small clearance $2a$ from 1 to 8 mm leads to a decrease in the critical speed from 250 to 170 km/h. Thus, both the effective stiffness and the small clearance of the hydraulic yaw damper have remarkable impacts on

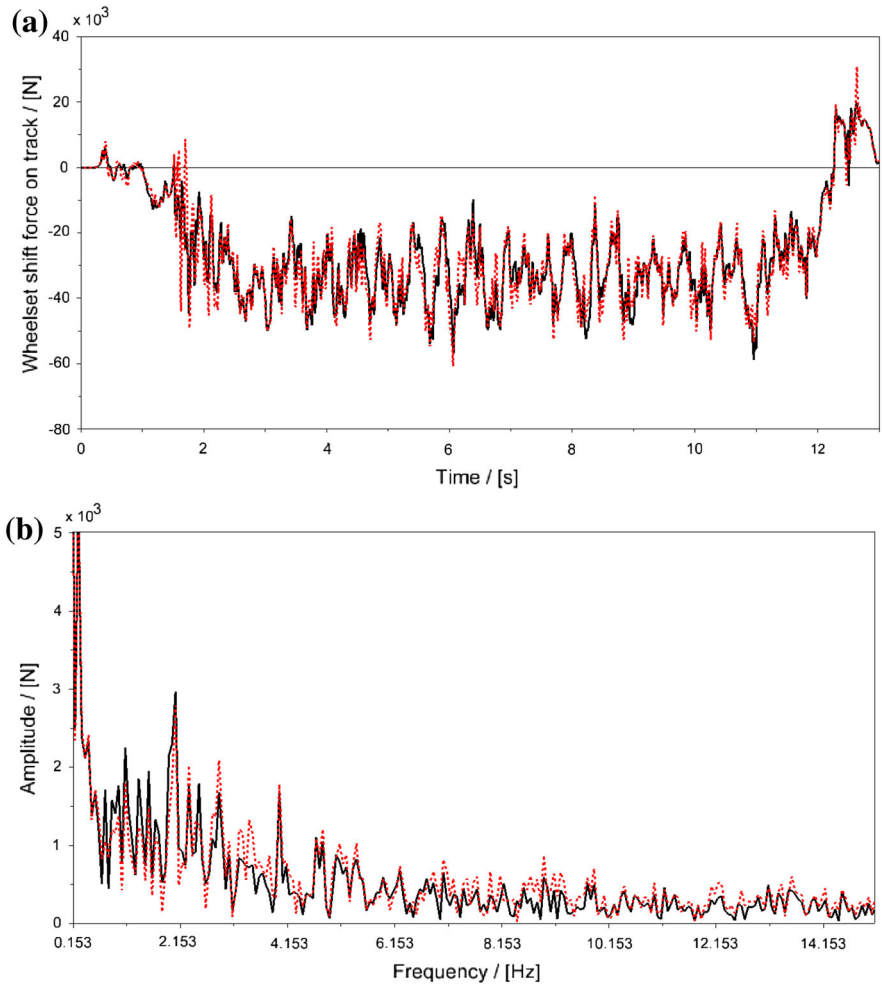

Fig. 19 Effect of small clearance variations in the hydraulic yaw damper on the No. 1 wheelset's lateral shift performance: **a** lateral shift force and **b** Bode plot of the lateral shift force (*black solid line* $2a =$ 0.5 mm, *red dotted line* $2a = 4$ mm; simulation conditions: $C_e =$ 1,000 kNs/m, $2a = 1$ mm, $V = 80$ km/h on a curved track, curve radius is 400 m and outer rail super-elevation is 0.12 m)

the locomotive's critical speed by a magnitude of 22–32 %, which obviously affects the locomotive's normal operation.

(2) Effective stiffness variation has a moderate influence on the locomotive's lateral ride index by a magnitude of approximately 3.5 %, but it has no obvious influence on the vertical ride index. A properly designed effective stiffness (i.e. not too soft or hard) is expected in design practice. Small clearance variations have an obvious influence on both the lateral and vertical ride indices of a locomotive, and increasing small clearance deteriorates both the lateral and vertical ride comforts.

The effect of small clearance on the locomotive's ride comfort, however, is more remarkable than that of effective stiffness. The small clearance not only couples lateral and vertical vibrations to some extent but also degrades the lateral and the vertical ride comforts by 9.2 and 14.2 %, respectively.

(3) Both the effective stiffness and the small clearance variations have hardly any influence on most of the locomotive's curve-negotiation indices, such as the derailment coefficient and wear power of the wheelsets. However, increasing the effective stiffness or small clearance increases the lateral shift force of the wheelsets to a limited extent.

(4) Other in-service parameter variations, such as that of oil temperature and entrained air ratio, indirectly affect a locomotive's dynamics by affecting the hydraulic yaw damper's effective stiffness and damping coefficient. A pertinent study shows that the effects of oil temperature and entrained air ratio on locomotive dynamics are neither obvious nor limited under normal conditions.

Small clearance and effective stiffness are usually omitted or simplified in engineering, and so it is important to use an improved in-service nonlinear damper model that considers series clearance and stiffness [1] in vehicle dynamics' studies and to improve the accuracy of vehicle design. It would also be practical to set pertinent vehicle maintenance engineering standards to control the influence of such in-service parameter variations.

Acknowledgments Financial supports from the open foundation (Grant No. 201308) of the State Key Laboratory of Fluid Power Transmission and Control in Zhejiang University and Hunan Provincial Natural Science Foundation (Grant No. 13JJ9037) of China are gratefully acknowledged.

Appendix

Parameters and values used in the MBS model of the SS_9 locomotive–rail coupling system

Notation (unit)	Description	Value	Remarks
M_c (kg)	Carbody mass	63400	
I_{cx} (kg m^2)	Carbody roll moment of inertia	143500	
I_{cy} (kg m^2)	Carbody pitch moment of nertia	1521000	
I_{cz} (kg m^2)	Carbody yaw moment of inertia	1718000	
H_c (m)	Vertical distance from the carbody's centre of gravity to rail top	2.1	
M_t(kg)	Bogie frame mass	20563	Includes the suspended mass of the primary suspension and unsprung mass of the secondary suspension
I_{tx} (kg m^2)	Bogie frame roll moment of inertia	7370	
I_{ty} (kg m^2)	Bogie frame pitch moment of inertia	73274	
I_{tz} (kg m^2)	Bogie frame yaw moment of inertia	78243	
H_t (m)	Vertical distance from the bogie's frame centre of gravity to rail top	0.9	
M_w (kg)	Wheelset mass	3239	Includes the unsprung mass of the primary suspension
I_{wx} (kg m^2)	Wheelset roll moment of inertia	2450	
I_{wy} (kg m^2)	Wheelset pitch moment of inertia	405	
I_{wz} (kg m^2)	Wheelset yaw moment of inertia	2450	
K_{px} (N/m)	Longitudinal stiffness of primary suspension	3.3E+007	Per axle side
K_{py} (N/m)	Lateral stiffness of primary suspension	4.0E+006	Per axle side
K_{pz} (N/m)	Vertical stiffness of primary suspension	2.15E+006	Per axle side
C_{pz} (Ns/m)	Vertical damping of primary suspension	80000	Per axle side (no damping in the bogie's centre axle)
K_{rubber_v1} (N/m)	Attachment stiffness of the primary vertical hydraulic damper	7.0E+006	Per damper (under normal conditions)
K_{sx} (N/m)	Longitudinal stiffness of secondary suspension	4.26E+005 (1.42E+005 for one spring)	Per bogie side
K_{sy} (N/m)	Lateral stiffness of secondary suspension	4.26E+005 (1.42E+005 for one spring)	Per bogie side
K_{sz} (N/m)	Vertical stiffness of secondary suspension	1.596E+006 (5.32E+005 for one spring)	Per bogie side
C_{yaw} (Ns/m)	Longitudinal damping of secondary suspension	1000000	Per damper (one damper per bogie side)

Notation (Unit)	Description	Value	Remarks
K_{rubber_yaw} (N/m)	Attachment stiffness of the hydraulic yaw damper	1.25E+007	Per damper (under normal conditions)
C_{sy} (Ns/m)	Lateral damping of secondary suspension	90000	Per damper (one damper per bogie side)
K_{rubber_h2} (N/m)	Attachment stiffness of the secondary lateral hydraulic damper	7.0E+006	Per damper (under normal conditions)
C_{sz} (Ns/m)	Vertical damping of secondary suspension	120000	Per damper (two dampers per bogie side)
K_{rubber_v2} (N/m)	Attachment stiffness of the secondary vertical hydraulic damper	8.0E+006	Per damper (under normal conditions)
K_{seat} (N/m)	Hydraulic damper mounting seat stiffness	2.8E+007	Refer to reference [30]
D_{w1} (m)	Diameter of new wheel	1.25	
D_{w2} (m)	Diameter of half-worn wheel	1.2	
D_{w3} (m)	Diameter of worn wheel	1.15	
M_{c0} (kg)	Locomotive servicing mass	126000	Allowable relative error of -1 to $+3$ %
M_{axle} (kg)	Axle load	21000	
V_r (km/h)	Locomotive rated running speed	99	
V_{max1} (km/h)	Locomotive maximum running speed	160	With half-worn wheels
V_{max2} (km/h)	Locomotive allowable running speed	170	With half-worn wheels
R_s (m)	Locomotive minimum safe curving radius	125	Vehicle speed $\leq$5 km/h
L_{coup} (m)	Centre distance between the front and rear couplers	22.216	
H_{coup} (m)	Vertical distance from coupler centre to rail top	0.88	
L_{total} (m)	Carbody length	21.596	
L_{frame} (m)	Carbody frame length	21.3	
W_{car} (m)	Carbody width	3.105	
H_{car} (m)	Locomotive height (vertical distance from pantograph mounting seat to rail top)	4.1325	
H_{max} (m)	Vertical distance from the car body's highest point to rail top	4.754	
H_{panto} (m)	Vertical distance from the highest point of the lifted pantograph to rail top	5.1–6.5	
L_{axle} (m)	Bogie axle distance	2.15 + 2.15	$C_0 - C_0$ axle style
L_{axle0} (m)	Distance from the first axle to the last axle of the locomotive	15.87	
$H_{traction}$ (m)	Vertical distance from the traction rod centre to rail top	0.46	
L_{half} (m)	Half of the distance between the carbody's front and rear side bearings	5.391	
W_{track} (m)	Track gauge	1.435	
M_r (kg/m)	Effective railroad mass	330	Includes the steel rails, sleepers and the vibration fraction of the roadbed

Notation (Unit)	Description	Value	Remarks
I_{rx} (kg m^2/m)	Effective railroad mass roll moment of inertia	10	
K_{ry} (N/m)	Effective railroad lateral stiffness	2.0E+007	Per rail side
C_{ry} (Ns/m)	Effective railroad lateral damping	4.9E+004	Per rail side
H_{rail} (m)	Vertical distance from the railroad's lateral suspension point to rail top	0.176	Refer to Fig. 2c
K_{rz} (N/m)	Effective railroad vertical stiffness	7.5E+007	Per rail side
C_{rz} (Ns/m)	Effective railroad vertical damping	9.4E+004	Per rail side
L_{rail} (m)	Distance between the two railroad vertical suspension points	1.508	Refer to Fig. 2c

References

1. Wang, W.L., Huang, Y., Yang, X.J., Xu, G.X.: Nonlinear parametric modeling of a high-speed rail hydraulic yaw damper with series clearance and stiffness. Nonlinear Dyn. **65**(1–2), 13–34 (2011)
2. Wickens, A.: Fundamentals of rail vehicle dynamics: guidance and stability. Swets & Zeitlinger Publishers, Lisse (2003)
3. Zhai, W.M.: Vehicle-track coupling dynamics. Science Press, Beijing (2007). (in Chinese)
4. Lee, S.Y., Cheng, Y.C.: Hunting stability analysis of high-speed railway vehicle trucks on tangent tracks. J. Sound Vib. **282**, 881–898 (2005)
5. Cheng, Y.C., Lee, S.Y.: Hunting stability analysis of a new high-speed railway vehicle model moving on curved tracks. In: ASME International Mechanical Engineering Congress and Exposition, pp. 1615–1624, Seattle, WA, USA (2007)
6. Zboinski, K., Dusza, M.: Self-exciting vibrations and Hopf's bifurcation in non-linear stability analysis of rail vehicles in a curved track. Eur. J. Mech. A **29**(2), 190–203 (2010)
7. Mohan, A., Ahmadian, M.: Nonlinear investigation of the effect of suspension parameters on the hunting stability of a railway truck. In: Proceedings of the IEEE/ASME Joint Rail Conference, pp. 327–336, Atlanta, GA, USA (2006)
8. Sayyaadi, H., Shokouhi, N.: A new model in rail-vehicles dynamics considering nonlinear suspension components behavior. Int. J. Mech. Sci. **51**(3), 222–232 (2009)
9. Suarez, B., Felez, J., Maroto, J., Rodriguez, P.: Sensitivity analysis to assess the influence of the inertial properties of railway vehicle bodies on the vehicle's dynamic behavior. Veh. Syst. Dyn. **51**(2), 251–279 (2013)
10. Fujimoto, H., Miyamoto, M.: Lateral vibration and its decreasing measure of a Shinkansen train. Veh. Syst. Dyn. **25**(suppl), 188–199 (1996)
11. Wrang, M.: Instability phenomena of a passenger coach, caused by internal yaw damper flexibility. Veh. Syst. Dyn. **33**, 406–417 (1999)
12. Mellado, A.C., Gómez, E., Viñolas, J.: Advances on railway yaw damper characterisation exposed to small displacements. Int. J. Heavy Veh. Syst. **13**(4), 263–280 (2006)
13. Piao, M.W., Kong, W.G., Liu, T., Zhao, W.Z.: Stability analysis of a high-speed bogie subject to anti-hunting damper failures. J. Dalian Jiaotong University. **32**(4), 1–5 (2011) (In Chinese)
14. Ahmed, A.S., Jalil, R.S.: A survey of rail vehicle track simulations and flexible multi-body dynamics. Nonlinear Dyn. **26**(2), 179–210 (2001)
15. Schupp, G.: Simulation of railway vehicles: necessities and applications. Mech. Des. Struct. **31**(3), 297–314 (2003)
16. Pérez, J., Busturia, J.M., Mei, T.X., Vinolas, J.: Combined active steering and traction for mechatronic bogie vehicles with independently rotating wheels. Annu. Rev. Control **28**, 207–217 (2004)
17. Zolotas, A.C., Pearson, J.T., Goodall, R.M.: Modelling requirements for the design of active stability control strategies for a high speed bogie. Multibody Syst. Dyn. **15**, 51–66 (2006)
18. Eom, B.G., Lee, H.S.: Assessment of running safety of railway vehicles using multibody dynamics. Int. J. Precis. Eng. Man. **11**(2), 315–320 (2010)
19. Schupp, G., Jaschinksi, A.: Virtual prototyping: the future way of designing railway vehicles. Int. J. Veh. Des. **22**(1–2), 93–115 (1999)
20. Stribersky, A., Moser, F., Rulka, W.: Structural dynamics and ride comfort of a rail vehicle system. Adv. Eng. Softw. **33**(7–10), 541–552 (2002)
21. Jalil R.S.: Accurate rail vehicle dynamic simulations by DynaRail. In: ASME International Mechanical Engineering Congress and Exposition, pp. 1–16, Anaheim, CA, USA (2004)
22. Wallrapp, O.: Review of past developments in multi-body system dynamics at DLR-from FADYNA to SIMPACK. Veh. Syst. Dyn. **41**(5), 339–348 (2004)
23. Eichberger, A., Hofmann, G.: TMPT: multi-body package SIMPACK. Veh. Syst. Dyn. **45**(suppl), 207–216 (2007)
24. European Standard: Railway Applications—Suspension Components—Hydraulic Dampers, CEN EN 13802 (2004)
25. Yu, W.B.: Shaoshan 9 electric locomotive. China Railway Publishing House, Beijing (2005). (in Chinese)
26. Wang, F.T., Zhou, J.S., Ren, L.H.: Analysis of track spectrum density for dynamic simulation of high-speed vehicles. J. China Railway, Society. **24**(5), 21–27 (2002) (in Chinese)
27. Li, J.B.: Irregularity power spectrum density analysis for speed-up tracks. Master's Degree Thesis, Tongji University, 2008 (in Chinese)

28. INTEC GmbH.: SIMPACK: Wheel/Rail Basic Training. INTEC GmbH, Wessling, Germany (2006)
29. Field Test Report: Dynamics performance field test report for SS_9 0001# electric locomotive. China Academy of Railway Sciences, Beijing (1999) (in Chinese)
30. Yang, X.J.: Module design of installation seat for yaw damper on locomotive car-body. Electr. Locomot. & Mass Transit. Veh. **28**(1), 18–20 (2005) (In Chinese)
31. Chinese Railway Society Standard: Evaluation methods and criteria for dynamics performance test of railway locomotives, TB/T 2360–93 (1993) (in Chinese)